Journal Name

ARTICLE

Peptide Metal-Organic Frameworks under pressure: flexible linkers for cooperative compression

Received 00th January 20xx,
Accepted 00th January 20xx

DOI: 10.1039/x0xx00000x

www.rsc.org/

José Navarro-Sánchez[a], Ismael Mullor-Ruíz[a,e], Catalin Popescu[b], David Santamaría-Pérez[c], Alfredo Segura[c], Daniel Errandonea[c], Javier González-Platas[d] and Carlos Martí-Gastaldo*[a]

We investigate the structural response of a dense peptide Metal-Organic Framework by using *in-situ* powder and single-crystal x-ray diffraction under high-pressures. Crystals of $Zn(GlyTyr)_2$ show a reversible compression by 13 % in volume at 4 GPa that is facilitated by the ability of the peptidic linker to act as a flexible string for a cooperative response of the structure to strain. This structural transformation is controlled by changes to the conformation of the peptide, that enables a bond rearrangement in the coordination sphere of the metal and changes to the strength and directionality of the supramolecular interactions specific to the side chain groups in the dipeptide sequence. Compared to other structural transformations in Zn(II) peptide MOFs, this behaviour is not affected by host/guest interactions and relies exclusively on the conformational flexibility of the peptide and its side chain chemistry.

Introduction

Metal-Organic Frameworks (MOFs) are crystalline, porous materials built from the interconnection of metal ions or clusters and organic linkers to produce porous architectures. Based on their unlimited chemical/structural versatility combined with the fine control over porosity metrics, MOFs found rapid application as storage media and selective sieve for gases like carbon dioxide (clean energy and environmental protection), methane and hydrogen (energy storage) or as heterogeneous catalysts.[1,2] These applications involve subjecting MOFs to chemical/physical pressure and mechanical stress, which demands for further understanding of their mechanical and structural response with applied pressure in order to optimize their performance. However, the number of works attempting to clarify this question remains still scarce. To date, most representative high-pressure crystallographic studies available include archetypical frameworks as HKUST-1,[3,4] zeolitic imidazolate frameworks (ZIF) –including the dense ZIF-4[5] and porous ZIF-8–,[6,7] MOF-5,[8] MIL-53,[9] UiO[10] and more recently the retrofitting studies in MOF-520.[11] All these works are exclusively based on MOFs built from rigid polyaromatic connectors. Hence, structural transformations are limited to relative displacement of organic and inorganic components of the net, contraction of coordination bonds or occasional tilting of the linker, which undergoes very small changes in its internal structure. Alternative linkers featuring a richer conformational landscape might result in more elastic frameworks for which the availability of multiple low-energy conformational states for the linker would enable reversible deformation under stress. [12] This is the case of oligopeptides based on short sequences of amino acids (aa's). Previous studies demonstrate that peptide MOFs feature unprecedented structural flexibility. They can accommodate their structure to environmental changes like solvent removal, guest exchange or pore filling with a manifold of responses that include: inelastic changes,[13] cooperative closure of porosity,[14] sponge-like behaviour,[15] guest inclusion[16] and adaptable porosity.[17]

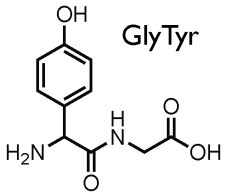

Scheme 1 Structure of glycyl-L-tyrosine (GlyTyr).

Although this structural adaptability is often ascribed to the torsional flexibility of the peptidic chain, the presence of sidechain non-coordinating groups in the backbone of the peptide capable of establishing supramolecular interactions might be equally important in directing structural transformations. The crystallographic studies available do not allow for easy discrimination between these two sources of changes to their structures. They are based exclusively on porous materials, for which framework/guest (solvent or gas molecules) interactions might be equally responsible for reversible changes in the structure. We hypothesised this could be better understood with high-pressure X-ray diffraction studies of a dense peptide MOF. The effect of high pressures over the compressibility of this family of materials remains still unexplored and this would allow for neglecting the effect of pore filling and the changes associated to guest inclusion, generally responsible for pressure-induced transformations. In this way, structural response would be limited only to internal changes in the framework associated to inter-peptide supramolecular interactions and peptide-metal coordination bonds, to enable direct evaluation of the elasticity of this type of connectors and the frameworks built from them.

[a] *Universidad de Valencia (ICMol), Catedrático José Beltrán-2, 46980, Paterna (Spain)*
[b] *CELLS-ALBA Synchrotron Light Facility, Cerdanyola, Barcelona 08290 (Spain)*
[c] *Departamento de Física Aplicada-ICMUV, Universidad de Valencia, MALTA Consolider Team, Edificio de Investigación, C/Dr. Moliner 50, 46100 Burjassot, Valencia (Spain)*
[d] *Departamento de Física, Universidad de La Laguna, 38204 La Laguna, Tenerife (Spain)*
[e] *Department of Bioengineering. Imperial College London. London SW7 2 AZ (United Kingdom)*
† E-mail: carlos.marti@uv.es
Electronic Supplementary Information (ESI) available: [details of any supplementary information available should be included here]. See DOI: 10.1039/x0xx00000x

Results and discussion

Synthesis and structure of $Zn(GlyTyr)_2$

$Zn(GlyTyr)_2$ (GlyTyr = glycyl-L-tyrosine; Scheme 1) was synthesised by solvothermal reaction of zinc(II) nitrate with enantiopure GlyTyr at 85 ºC in a mixture of methanol and toluene. Controlled cooling results in the quantitative formation of colourless, prismatic crystals with sizes close to 50 µm (Figure SI2). $Zn(GlyTyr)_2$ crystallizes in the monoclinic, polar, space group *I*2. Homochirality is confirmed by the Flack parameter value of 0.014(13) (Table SI1). It is built from the four-fold coordination of Zn(II) centers by C-terminal Tyr carboxylate groups and N-terminal Gly amino groups of two GlyTyr molecules. These last act as bridges to form a neutral grid-like layer (Figure 1a). The internal structure of this layer is reminiscent of other peptide-based porous materials like $Zn(GlyAla)_2$, [17] $Zn(GlySer)_2$ [14] or $Zn(GlyThr)_2$[13] (Figure SI7). However, the solid packs into a dense structure with no empty space available for accommodating solvent molecules (Figure 1b). Packing is controlled by H-bonding interactions between neighbouring layers that interleaves them to produce a non-porous solid. As shown in Figure 1c, supramolecular interactions involve the phenol units specific to the aa Tyr (O3) and the C=O (O4) and NH (N1) groups from the peptide bond (Table SI2). As suggested by previous examples,[13,14,16,17] this highlights the importance of sidechain chemistry in directing the structure of metal-peptide coordination polymers. The structure of $Zn(GlyTyr)_2$ makes it ideal to study the intrinsic elasticity of the dipeptide connector with external pressure. Besides neglecting the effect of host/guest interactions over the structural response of the solid, the absence of solvent is also expected to simplify the refinement of High-Pressure X-Ray Diffraction (HP-XRD) data.

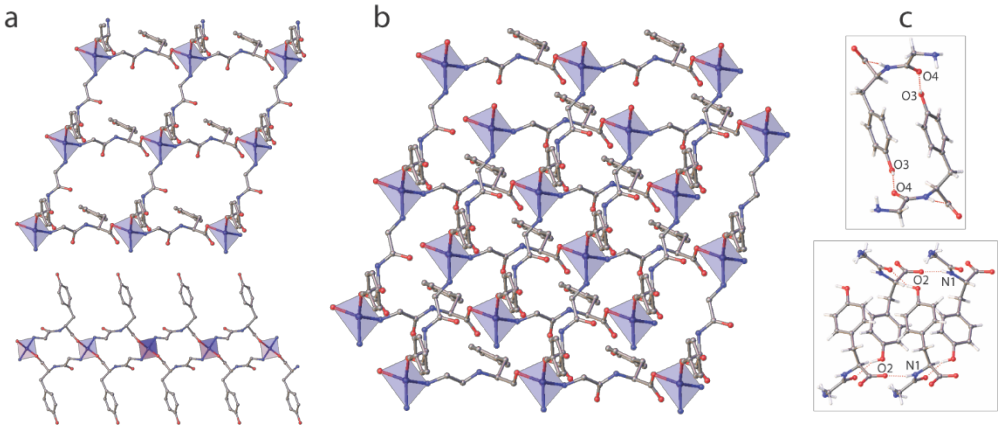

Fig.1 Structure of $Zn(GlyTyr)_2$. a) View of the peptide metal grid-like layer along [1 1 1] (top) and [0 1 0] (bottom) directions. b) The solid crystallizes as a dense material due to interweaving of neighbouring layers. c) Packing is controlled by inter-layer H-bonding interactions specific to the Tyr sidechain (top) and the peptide bond (bottom).

High-pressure powder X-ray Diffraction and effect of the pressure transmitting medium

Previous works suggest that the Pressure Transmitting Medium (PTM) used for hydrostatic regime affects the structural response and amorphization pressure of metal-organic hybrids. [4,10,18] In order to define which was the most suitable medium to enable high-quality data collection at high-pressures whilst avoiding amorphization, we first carried out powder XRD experiments. As shown in SI2, phase purity of the bulk material was first confirmed by CHN, FT-IR, Scanning Electron Microscopy (SEM), thermogravimetric analysis and powder X-ray diffraction (PXRD). Homochirality was also confirmed with circular dichroism (CD), that presents a negative Cotton effect in the UV-Vis spectrum of the below 300 nm due to Zn(II) complexation with enantiopure glycil-L-tyrosine (Figure SI6). Polycrystalline samples and ruby crystals, for pressure calibration, were loaded into a gasketed Diamond Anvil Cell (DAC) equipped with a 500 µm diamond culet. Next, in different experiments, they were immersed in Fluorinert (FC-70), methanol, ethanol, dimethylformamide (DMF) and a mixture of methanol and water (3:1 in volume) as quasi hydrostatic liquids. HP powder diffraction was collected on increasing pressures up to a maximum of 8 GPa and then back to ambient pressure for reference. For all of them we found a qualitatively similar behaviour. Bragg peaks evolve towards higher angles under compression with different pressure dependences, which is a consequence of the anisotropic compression of the solid. As result, a few peaks merge under compression and others, like [100] and [-401], split. There is no evidence of the pressure media penetrating into the MOF. There are some changes in the relative intensities of Bragg peaks due to preferential orientations, which get amplified because of the focused X-ray beam used. All the experiments show a broadening of the diffraction beyond 4 GPa due

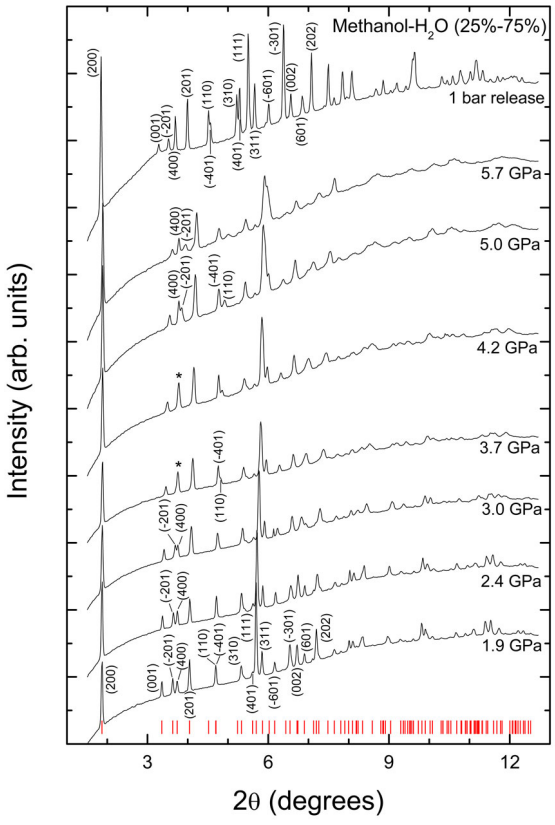

Fig. 2 HP-PXRD of $Zn(GlyTyr)_2$ in methanol:water (3:1). The merging of the diffraction lines [-201] and [400], that stands for anisotropic compression, is highlighted.

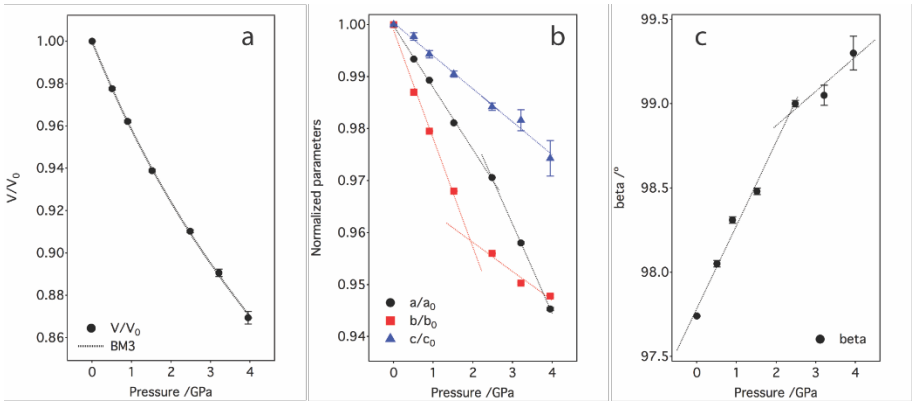

Fig.3 HP cell contraction of single-crystals of Zn(GlyTyr)2 in methanol:ethanol:water. a) Unit cell volume compression with pressure. Dashed line stands for the EoS model fit. Error bars are smaller than their respective size symbols. b) Evolution of the unit cell parameters and c) beta angle with increasing pressure showing a discontinuity above 2 GPa. Solid lines are only a guide to the eye.

to the deterioration of quasi-hydrostatic conditions of the different PTMs used. [19,20] However, crystallinity is retained up to the highest pressure covered by the experiments. The peaks broadening was more acute for the experiments performed in MeOH, EtOH and DMF (Figure SI8-10). In turn, the quality of the PXRD patterns in FC-70 (Figure SI11) and MeOH:H_2O (Figure 2) experiments is comparatively higher, suggesting that these were the more adequate PTMs for single-crystal studies. This last shows an anisotropic compression that accounts for the differential pressure evolution of Bragg peaks. This is confirmed by the merging of [-201] and [400] into one peak at 3.7 GPa and their inversion from low to high pressures. All the changes observed were reversible upon pressure release.

High-pressure structural transformation in a single crystal

With this information in hand we decided to analyse the effect of pressure in a single-crystal for more precise structural information. Figure 3a represents the evolution of the volume cell of $Zn(GlyTyr)_2$ in MeOH:EtOH:H_2O (16:3:1) on increasing pressure. The unit cell shows a continuous compression down to 87 % of the original value at 3.95 GPa, while remaining crystalline. It is worth noting that this variation is equivalent to the reversible compression described above for the polycrystalline solid by using MeOH:H_2O as PTM (Figure SI14). This denotes a resilient material with a large pressure response that lies close to the maximum volume changes reported for other molecule-based crystalline materials like ZAG-4 (27%, 7 GPa) [18] or the family LnFe(CN6) (20%, 1GPa). [21] We used the EosFit7-GUI program [22] to calculate the equation of state (EoS) by using a third-order Birch-Murnaghan function (Figure SI14, Table SI3). This provides a value of V_0 of 1082.00(6) Å3 and a bulk modulus of K_0 = 21.9(9) GPa and K´= 4.2(8). All refinements of EoS yield $\omega\chi^2$<1 due to over-estimation of $\sigma(P)$, but none of the fits show any systematic variation of P_{obs}-P_{calc} with pressure, ensuring that the calculated parameters are consistent with the experimental data. For comparison, molecular solids generally present bulk moduli below 30 GPa. [23] In particular, MOFs often present a lower resistance to compression that scales down with increasing porosity and lower density. Although higher K values have been reported, these are not directly related to the compression of the framework but to the penetration of the PTM into the pores that increases the stability of the system at low-P regimes. [24] When it comes to non-porous (dense) MOFs, the compressibility of Zn(GlyTyr)2 is substantially higher than those reported for very stable zeolite-type materials like Zn(Im)2-zni (14 GPa) [23] and LiB(Im)4 (16.6 GPa). [25] Also, these last display smaller changes in the volume cell at the higher pressures studied (below 10%).

The evolution of unit cell parameters upon compression is different to that of the unit cell volume (Figure 3b). The curves show a slope change above 2 GPa that suggests a possible phase transition. We argue this can be classified as an isostructural second-order phase transition as there is no change in the space group and the compression of the cell volume does not show any discontinuity in the range of pressures evaluated. To our surprise, apart from decreasing diffraction intensity, this transformation takes place without compromising the integrity of the crystal thus enabling

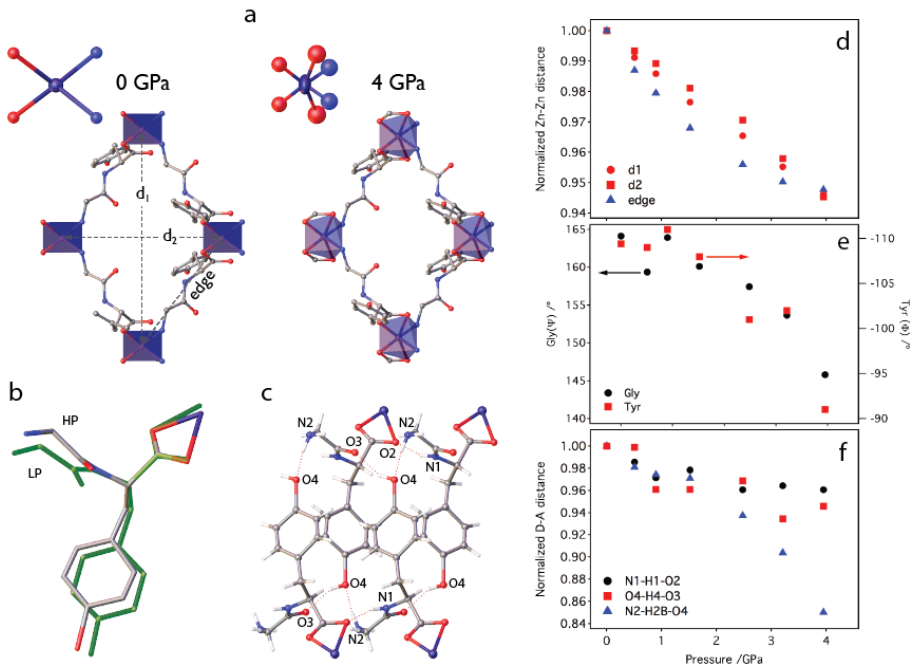

Fig. 4 Structural changes in Zn(GlyTyr)2 at high-pressure. Comparison of the structure at 0 and 4 GPa to show changes in: a) Coordination geometry and internal structure of the grid-like layer along [101]. Variations in the distance separating Zn(II) has been measured for the edge and diagonals (d1 and d2) of the rhomboid; b) Changes to the peptide conformation. For clarity, LP phase is highlighted in green and c) Formation of additional H-bonds at 4 GPa. Evolution of the most relevant structural parameters with pressure: d) Zn-Zn distance, e) Peptide internal dihedral angles (Ψ and Φ) and f) Selected H-bond distances along [100]. For clarity, changes have been normalized to the value at room pressure. See Table SI5 for the absolute values.

refinement of all data sets for precise structural information. As earlier suggested by HP-PXRD experiments, $Zn(GlyTyr)_2$ displays a highly anisotropic resistance to compression. As shown in Figure SI16, the direction [-101] displays a high resistance to the compression for negligible changes close to 1 % due to high density of atoms in this direction while the softest compression takes place along in [010] direction (or [101] after 3 GPa) on account of reorganization of phenyl rings and therefore pi-pi interactions and some hydrogen bonds. This is often observed for layered covalent crystals, for which intralayer distances are less compressible than those between layers.[26] Figure 4 summarises the most characteristic changes to the structure of the peptide MOF with pressure. The phase transition proceeds via cooperative bond rearrangement in the coordination sphere of Zn(II) centers controlled by the coordination mode of the C-Term Gly carboxylate group, that evolves from four-fold distorted trigonal pyramidal (η^1) at room pressure into a six-fold distorted trigonal prismatic geometry (η^2). As pointed out before, according to our HP-PXRD data (Figure SI12), this transformation proceeds reversibly. This change to the overall connectivity of the network is not isolated and proceeds upon the relaxation of the structure. This is enabled by cooperative changes to the internal structure of the layers, the conformation of the dipeptide and adjustments to the directionality and strength of interlayer supramolecular interactions. As shown in Figure 4a and 4d, the grid-like layers feature an isotropic compression. The edge and diagonal distances (d_1 and d_2) separating the metal nodes display an equivalent compression regime and decrease close to 6 % of the original value. This is coupled to a change in the dihedral angles of the peptide backbone. Ψ shows a clear closure trend from 164.1(3) to 146(6)º whereas Φ changes from -109.4(3) to -91(8)º. This suggests that the response of the linker to stress is controlled by the cooperative rotation of the two amino acids in the peptide. The solid also shortens the H-bond distances that dictate the interlayer separation for accommodating the change in pressure. This results in a compression of the bonds O4···O3 and N1···O2 down to 2.50(9) and 2.72(6) Å for a change of 3.9 and 5.4 %, respectively (Figure 4f). More important is the formation of an additional H-bond N2···O4 between the nitrogen in the amide bond and the –OH group in Tyr that becomes relatively strong (2.54(14) Å) after compressing close to 15 % of its original value (Figure 4c, Table SI5). This highlights the importance of supramolecular interactions in controlling cooperative changes in peptide MOFs. Just like $Zn(GlySer)_2$, in which the –OH groups intrinsic to Ser are key to enable cooperative closure of the structure upon formation of intralayer H-bonds,[14] the phenol units in Tyr seem to play an important role in relaxing the structure and retaining crystallinity up to very high pressures. As for the π-π interactions between neighbouring units, we also identify a clear decrease in the distance separating the aromatic rings in Tyr (Figure SI18). However, they are not short enough to consider them to play an important role in directing the structural transformation.

Conclusions

In summary, we have carried out a crystallographic study to unveil the structural response of peptide MOFs to high-pressures for the first time. Crystals of $Zn(GlyTyr)_2$ can be compressed reversibly by 13 % in volume at 4 GPa, whilst maintaining long-range order. The peptide, acting as metal connector, behaves as a flexible string and facilitates a cooperative response of the structure to mechanical strain. The relaxation of the structure is controlled by the internal rotation of the two amino acids in the peptide that modify its conformation and trigger a bond rearrangement at the coordination sphere of the metal coupled to changes in the strength and directionality of H-bonds. Overall, the landscape of conformations accessible to the peptide combined with the directional nature of non-covalent interactions provides a compressible cushion that allows for accommodating large distortions in the framework whilst avoiding amorphization. Compared to other structural transformations reported for peptide MOFs based on tetrahedral Zn(II) nodes, [14] this behaviour is not affected by host/guest interactions and relies exclusively on the conformational flexibility of the peptide and its side chain chemistry.

Conflicts of interest

There are no conflicts to declare.

Acknowledgements

This work was supported by the EU (ERC Stg Chem-fs-MOF 714122, FEDER funds) and Spanish MINECO (MDM-2015-0538, MAT2015-71070-REDC, MAT2016-75586-C4-4-P, MAT2016-75586-C4-1-P & CTQ2017-83486-P). C.M.-G. and D.S.-P. thank the Spanish MINECO for a Ramón y Cajal Fellowship. J.G.-P. thanks to X-ray General Service (SIDIX) at La Laguna University. HP experiments were performed at the MSPD beamline at ALBA Synchrotron with the collaboration of in-line staff.

Notes and references

1 H. Furukawa, K. E. Cordova, M. O'Keeffe and O. M. Yaghi, *Science*, 2013, **341**, 1230444–1230444.
2 K. Adil, Y. Belmabkhout, R. S. Pillai, A. Cadiau, P. M. Bhatt, A. H. Assen, G. Maurin and M. Eddaoudi, *Chem. Soc. Rev.*, 2017, **46**, 3402–3430.
3 A. Graham, J. Tan and D. Allan, *Chem. Commun.*, 2012, **48**, 1535–1537.
4 K. W. Chapman, G. J. Halder and P. J. Chupas, *J. Am. Chem. Soc.*, 2008, **130**, 10524–10526.
5 T. D. Bennett, P. Simoncic, S. A. Moggach, F. Gozzo, P. Macchi, D. A. Keen, J.-C. Tan and A. K. Cheetham, *Chem. Commun.*, 2011, **47**, 7983–7985.
6 C. L. Hobday, T. D. Bennett, D. Fairen-Jimenez, A. J. Graham, C. A. Morrison, D. R. Allan, T. Düren and S. A. Moggach, *J. Am. Chem. Soc.*, 2018, **140**, 382–387.
7 S. A. Moggach, T. D. Bennett and A. K. Cheetham, *Angew. Chem. Int. Ed.*, 2009, **48**, 7087–7089.
8 A. J. Graham, D. R. Allan, A. Muszkiewicz, C. A. Morrison and S. A. Moggach, *Angew. Chem. Int. Ed.*, 2011, **50**, 11138–11141.
9 P. Serra-Crespo, E. Stavitski, F. Kapteijn and J. Gascon, *RSC Adv.*, 2012, **2**, 5051–5053.
10 C. L. Hobday, R. J. Marshall, C. F. Murphie, J. Sotelo, T. Richards, D. R. Allan, T. Düren, F.-X. Coudert, R. S. Forgan, C. A. Morrison, S. A. Moggach and T. D. Bennett, *Angew. Chem. Int. Ed.*, 2016, **128**, 2447–2451.
11 E. A. Kapustin, S. Lee, A. S. Alshammari and O. M. Yaghi, *ACS Cent. Sci.*, 2017, **3**, 662–667.
12 A. Worthy, A. Grosjean, M. C. Pfrunder, Y. Xu, C. Yan, G. Edwards, J. K. Clegg and J. C. McMurtrie, *Nat. Chem.*, 2017, **20**, 5834.

13 C. Marti-Gastaldo, J. E. Warren, K. C. Stylianou, N. L. O. Flack and M. J. Rosseinsky, *Angew. Chem. Int. Ed.*, 2012, **51**, 11044–11048.

14 C. Martí-Gastaldo, D. Antypov, J. E. Warren, M. E. Briggs, P. A. Chater, P. V. Wiper, G. J. Miller, Y. Z. Khimyak, G. R. Darling, N. G. Berry and M. J. Rosseinsky, *Nat. Chem.*, 2014, **6**, 343–351.

15 C. Martí-Gastaldo, J. E. Warren, M. E. Briggs, J. A. Armstrong, K. M. Thomas and M. J. Rosseinsky, *Chem-Eur J.*, 2015, **21**, 16027–16034.

16 A. P. Katsoulidis, K. S. Park, D. Antypov, C. Martí-Gastaldo, G. J. Miller, J. E. Warren, C. M. Robertson, F. Blanc, G. R. Darling, N. G. Berry, J. A. Purton, D. J. Adams and M. J. Rosseinsky, *Angew. Chem. Int. Ed.*, 2014, **53**, 193–198.

17 J. Rabone, Y. F. Yue, S. Y. Chong, K. C. Stylianou, J. Bacsa, D. Bradshaw, G. R. Darling, N. G. Berry, Y. Z. Khimyak, A. Y. Ganin, P. Wiper, J. B. Claridge and M. J. Rosseinsky, *Science*, 2010, **329**, 1053–1057.

18 K. J. Gagnon, C. M. Beavers and A. Clearfield, *J. Am. Chem. Soc.*, 2013, **135**, 1252–1255.

19 M. J. P. Brugmans and W. L. Vos, *J. Chem. Phys.*, 1998, **103**, 2661–2669.

20 S. Klotz, J. C. Chervin, P. Munsch and G. Le Marchand, *J. Phys. D: Appl. Phys.*, 2009, **42**, 075413.

21 S. G. Duyker, V. K. Peterson, G. J. Kearley, A. J. Studer and C. J. Kepert, *Nat. Chem.*, 2016, **8**, 270–275.

22 J. Gonzalez-Platas, M. Alvaro, F. Nestola and R. Angel, *J. Appl. Cryst.*, 2016, **49**, 1377–1382.

23 E. C. Spencer, R. J. Angel, N. L. Ross, B. E. Hanson and J. A. K. Howard, *J. Am. Chem. Soc.*, 2009, **131**, 4022–4026.

24 S. C. McKellar and S. A. Moggach, *Acta Crystallogr. Sect. B Struct. Sci.*, 2015, **71**, 587–607.

25 T. D. Bennett, J.-C. Tan, S. A. Moggach, R. Galvelis, C. Mellot-Draznieks, B. A. Reisner, A. Thirumurugan, D. R. Allan and A. K. Cheetham, *Chem-Eur J.*, 2010, **16**, 10684–10690.

26 D. Errandonea, D. Martínez-García, A. Segura, J. Haines, E. Machado-Charry, E. Canadell, J. C. Chervin and A. Chevy, *Phys. Rev. B*, 2008, **77**, 045208.